The Dynamics of *Cryptococcus neoformans* infection in *Galleria mellonella*

Daniel F. Q. Smith[a], Aviv Bergman[b,c], and Arturo Casadevall[a]#

[a] Department of Molecular Microbiology and Immunology, Johns Hopkins School of Public Health, Baltimore, Maryland, USA

[b] Department of Systems and Computational Biology, Albert Einstein College of Medicine, New York City, New York, USA

[c] Santa Fe Institute, Santa Fe, New Mexico, USA

Running Head: Timelapse recording of fungal infections in *G. mellonella*

#Address Correspondence to Arturo Casadevall, acasade1@jh.edu

Abstract Word Count: 189

Text Word Count: 3,502

Abstract

Galleria mellonella has emerged as an important host for the study of fungal virulence, insect immune responses, and the evaluation of antifungal agents. In this study we investigated the dynamics of fungal infections in *G. mellonella* using *Cryptococcus neoformans*, a human pathogenic fungus. Since the analysis of infection dynamics requires a fine temporal resolution of larval death, we employed a photographic timelapse technique that allowed us to simultaneously measure death by proxy of larval melanization and absence of movement. Larval mortality occurred in two phases, early and late, which differed in their timing of melanization. Early phase deaths occurred with rapid whole-body onset of melanization, followed by sudden cessation of movement several hours later. Contrastingly, late phase deaths occurred with a gradual cessation of movement, followed by melanization, typically radiating from one location on the larva. The differences in mortality kinetics suggests differences in fungal pathogenesis with one population succumbing early while the rest linger for later death. Subsequent analysis of mortality data using the inversion method revealed predictable deterministic dynamics without evidence for chaotic signatures, indicating that this *C. neoformans-G. mellonella* infection model behaves differently than bacterial-insect models.

Importance

The ability to predict the course of an infection is critical to anticipating disease progression and effectively treating patients. Similarly, the ability to make predictions about pathogenesis in laboratory infection models could further our understanding of pathogenesis and lead to new treatments. As fungal diseases are expected to rise, understanding the dynamics of fungal infections will be important to anticipate and mitigate future threats. Here, we developed a timelapse method to visualize infections of *Galleria mellonella* larvae with the fungal pathogen *Cryptococcus neoformans*. This method provided insight into infection progression that are not apparent from standard survival measurement protocols, including the relationship

between melanization and death. Further, it enabled us to explore the dynamics of disease progression in this system, which revealed deterministic dynamics without evidence of chaos, implying predictability in the outcome of cryptococcal infection in this moth.

46 **Introduction**

47 Interactions between hosts and microbes vary greatly between host species, microbial
48 species, and specific circumstances of the interaction. Even when comparing the outcome of
49 interactions of the same host and microbial species in different experiments or situations,
50 changes in experimental conditions (i.e. microbial inoculum, temperature, or state of the hosts'
51 immune systems) can have major effects on pathogenic potential, symptoms of disease, and
52 the outcome of infection (1, 2). A host infected with a microbe at a certain inoculum might be
53 able to clear the infection readily, while a host exposed to the same inoculum but with a slightly
54 different immune response might launch a host-damaging inflammatory response to the
55 microbe, or might fail to clear the infection, resulting in microbial growth and host death.
56 Hence, damage can come from both the host immune response and microbial action (1).
57 Understanding the sources of variability in the outcome of host-microbe interactions is
58 important for improving reproducibility, anticipating future threats and developing improved
59 therapies for infectious diseases.

60 A fundamental question in the field of infectious diseases is the predictability of host-
61 microbe interactions. To know whether the host-pathogen interactions variables are
62 predictable, one must first determine whether the dynamics of the system, which can be either
63 random (stochastic) or non-random (deterministic). The outcome in random dynamics is not
64 predictable. For non-random or deterministic dynamical systems, one must further
65 differentiate whether it is chaotic (non-predictable) or non-chaotic (predictable). Predictability
66 would facilitate understanding and treatment of infections, because given certain parameters,
67 clinicians could effectively predict the trajectory of pathogenesis and mitigate it. If the host-
68 microbe interactions are chaotic, it means that while there are non-random variables at play,
69 the system is too dependent on the initial conditions, which implies non-predictability.
70 Mathematical chaos is typified in popular culture by the metaphor of the "butterfly effect,"

71 when seemingly insignificant actions or variables (i.e. a butterfly flying), can lead to
72 unpredictable and significant changes in larger and distant systems (I.e. altered weather
73 patterns). While chaotic systems, such as weather, are amenable to short term predication, the
74 countless minuscule, yet inevitably significant variables, cause downstream effects that long
75 term prediction impossible. If a host-microbial system is chaotic in a manner like weather
76 systems, understanding the important inputs of to the chaotic host-microbe interactions can
77 allow the creation of prediction models in a manner similar to modern meteorology. Chaos also
78 affects the reproducibility of experiments, a timely topic given concerns about the
79 reproducibility of results in the biomedical sciences (3).

80 A prior study of host-microbe dynamics used bacterial infection of invertebrate model
81 hosts (4). That study found evidence of chaos in the lifespan of insects and helminths infected
82 with *Pseudomonas s*pp., but not in the lifespan of control uninfected organisms. While bacteria
83 are important pathogens that affect hosts across kingdoms of life, that study did not include
84 fungal infections. Using different methodology and low sample size, *C. neoformans* infection in
85 *Galleria mellonella* wax moth larvae was found to be deterministic without evidence for chaos
86 (5). Comparing bacterial and fungal infections is important because fungi exhibit different
87 strategies for pathogenesis and differ from bacteria in their dependence between their
88 pathogenic potential and inoculum. Bacteria, which largely cause disease through the release of
89 toxins into the host, kill hosts in a direct inoculum-dependent manner according to measures of
90 pathogenic potential (6). Contrastingly, fungi, which cause disease largely through survival and
91 growth in the host, do not kill in a directly dose-dependent manner; rather, there is a
92 logarithmic relationship where the order of magnitude of inoculum leads to higher death and
93 measures of pathogenic potential (6). This implies different strategies for bacterial and fungal
94 pathogenesis that might be reflected in the dynamics of their interaction

95 A widely used system for the study fungal pathogenesis is the *Galleria mellonella* wax
96 moth model (7–12). *G. mellonella* allow for easy screening of virulence of different fungal
97 isolates or mutants, in a high-throughput and relatively rapid, easy, and affordable manner due
98 to fast infection timelines and easy availability of the organism. Here we used *C. neoformans*
99 infection in *G. mellonella* to explore the dynamics of animal fungal infection. We developed a
100 timelapse imaging protocol to track *G. mellonella* larval survival at a much higher resolution of
101 time intervals than is traditionally used (15 minutes versus 24 h). Using this system we found no
102 evidence for chaotic signatures in this model.
103

104 **Results/Discussion**

105 There are three current limitations with the collection of survival data in the *G.*
106 *mellonella* model for the purpose of studying infection dynamics. The first is the lack of
107 temporal resolution for the death event, since this is usually measured when the experimenter
108 checks the larvae. and it is not logistically feasible to achieve near continuous monitoring. The
109 second is that death is determined by manually checking the movement of the larvae at each
110 time interval, which usually involves physical stimulation of the larvae with a pipette tip, which
111 stresses the animal and could affect the results. Third is the need to collect hundreds of survival
112 data points for sufficient statistical power needed for the chaos calculations. To help overcome
113 these limitations, we developed a survival monitoring model that allowed frequent survival
114 measurements and removed the necessity of manual probing to ascertain whether the animal
115 was alive or dead. Specifically, we assembled timelapse cameras to record the movement of *G.*
116 *mellonella* larvae following infection within 24-well plates, with one larva per well. This allowed
117 each larva to be individually monitored at increments of 15 minutes. We analyzed the
118 timelapse movie frames and recorded the time at which movements of the larvae ceased as
119 well as the time in which melanization began to spread through the larvae's bodies. Larval

120 melanization results from the production of melanin pigment, which is part of the insect
121 immune response, and is associated with imminent or recent larval death (13–15).
122 The time lapse photography setup allowed us to study the kinetics of infected larva
123 melanization relative to the cessation of movement (Supplementary Video 1). We first
124 compared cessation of movement as measured by time lapse photography to the accepted
125 method of manual larval poking for establishing death (Figure 1A). The photography and
126 manual poking survival curves closely paralleled one another but there was an approximate 1-
127 day lag in mortality as measured by cessation of movement, implying that some of immobile
128 larvae could be roused to move if poked. The fact that cessation of movement was highly
129 correlated with eventual demise we accepted this difference in mortality timing because it
130 eliminated mechanical poking, which could potentially introduce a set of new variables ranging
131 from stress to operator variability and renders high temporal resolution almost impossible. We
132 experimented with placing larvae in 12- and 24-well plates. The attraction of the 24-well plate
133 was that it would allow us to image a larger number of larvae per experiment. However, larvae
134 placed in 24-well plates died before those in 12-well plates (Figure 1B). Although this
135 phenomenon was not further investigated it could reflect additional stress from confinement in
136 a small space. Alternatively, reducing space would reduce their space for movement, which is
137 necessary for hemolymph circulation. regardless, we settled on using 24-well plates even
138 though this reduced our experimental survival time.
139 Next, we used time lapse photography to evaluate the dynamics of cryptococcal
140 infection in this host. *G. mellonella* survival after a high inoculum infection with *C. neoformans*
141 manifested two distinct phases, one concluding by 48 h (Supplementary Video 2) and the other
142 starting gradually at about 96 h (Supplementary Video 3) and continuing till the end of the
143 experiment when all the larvae died (Figure 2A). Melanization preceded the cessation of
144 movement during the first phase generally followed the cessation of movement during the

145 second later phase (Figure 2A). With control larvae that died following PBS injection, which
146 presumably reflect trauma, death in these controls occurred later than the deaths from *C.*
147 *neoformans* infection, and the time between melanization and cessation of movement was
148 closely linked. When the same survival data were rounded to the nearest 24-h increment, as
149 would be the case with the standard daily manual survival measurements, we see that this two-
150 phase curve is lost due to the reduced temporal resolution (Figure 2B). This indicates that some
151 patterns of host survival and clues to underlying pathogenesis are usually lost due to standard
152 survival assay methodology based on recording events at discrete time intervals.
153 Melanization in *G. mellonella* larvae was measured by quantifying the mean gray value
154 of the individual wells containing the larvae. Melanization causes the larvae to become darker
155 and thus the mean gray value of the well becomes lower since lower gray values denote darker
156 pixels. When looking at the melanization response we noticed that early phase larvae
157 melanized rapidly and uniformly throughout their bodies, approximately 5-10 h prior to the
158 cessation of movement (Figure 3A, B, C, E). Larval melanin reached a brief plateau immediately
159 prior to the cessation of movement (Figure 3C, red arrows), followed by more melanization.
160 Conversely, the larvae that died later had melanization start in one spot of their body and then
161 spread (Figure 3A, D, E). This spot was usually either at the head or the posterior end, in a
162 location in the body cavity not necessarily associated with the site of injection. The
163 melanization reaction then spread slowly from these spots and/or from the head of the larvae
164 for several hours after the larvae stopped moving (Figure 3E). The white arrow indicates where
165 melanization began and radiated from, in addition to the head of the organism (Figure 3E). This
166 again suggests two mechanisms of pathogenesis during infection. The rapid and complete onset
167 of melanization in the early death phase indicates a systemic melanization response in the
168 hemolymph of the larvae. Since melanin synthesis is the result of a polymerization reaction that
169 yields highly reactive and toxic intermediates, melanization prior to death suggests the

170 possibility that this immune mechanism is contributing to the demise of the larvae. In contrast,
171 the focal melanization in the later phase could reflect melanization within a large immune
172 nodule (16) – a complex of immune cells, clotting factors, melanization factors, and other
173 immune components aimed at restricting and killing microbes. One interpretation of these
174 results is that early deaths occur when the fungus is dispersed throughout the hemolymph
175 triggering widespread melanization, while later deaths reflect following dissemination from an
176 infected tissue or an immune nodule that is no longer able to contain the fungal infection.

177 To examine the dynamics of the *C. neoformans-G. mellonella* interaction, we applied the
178 inversion measure to the observed time distributions. This approach allowed us to assess
179 deviations from expected stochastic patterns by comparing our empirical data to a null
180 hypothesis of non-chaotic behavior. Our analysis did not yield statistically significant evidence
181 to reject the null hypothesis ($p \geq 0.2$) (Figure 4A), suggesting that, within the resolution of our
182 dataset and analytical framework, there is no strong indication of chaos governing the observed
183 host-pathogen interactions. Given that our observations were taken at 15 min, deaths recorded
184 at a given time point must have reflected events occurring within that time interval. To account
185 for this impreciseness in knowing the timing of the event, we randomly assigned observed
186 deaths across smaller subintervals within that interval, introducing randomness into the
187 analysis. While this approximates the likely times of death, it could also obscure any chaotic
188 signature. Consequently, rather than calculating a single inversion measure for the histogram,
189 we generated a distribution of inversion measures and compared it to the null bootstrap
190 distribution. No statistically significant difference was found between the sample and the
191 bootstrap null distributions ($p = 0.5$) (Figure 4B). This results are consistent with a prior
192 analysis of the dynamics of *C. neoformans-G. mellonella* interactions using different analytic
193 methods that also found no chaos in this system (5).

194 The absence of chaotic signatures in this system differs from evidence of chaos in
195 *Pseudomonas* spp. infections of flies and worms (4). We do not know whether this reflects a
196 fundamental difference between bacterial and fungal infections, is a consequence of using a
197 different host, a different method of infection or another aspect of the experimental
198 inoculation. Since bacteria differ from fungi in mostly kill their host in a linear and logarithmic
199 inoculum-dependent manner, respectively (6), it is possible that the difference in dynamics
200 reflects an intrinsic difference between these microbial types. . An additional difference
201 between this study and the prior bacterial studies is that those infections were acquired
202 through natural inoculation through ingestion by the host. In contrast, in this study we injected
203 larvae with the inoculum directly since there is no practical means of inducing a natural
204 cryptococcal infection in *G. mellonella*. Hence, our approach involved piercing the larval surface
205 with a needed and delivering the inoculum to deeper tissues, which could produce a non-
206 chaotic deterministic outcome by causing a fulminant infection that abrogates chaotic
207 signatures. Future studies will have to dissect these possibilities to determine whether fungal
208 infections show signs of mathematical chaos or whether the reason for the lack of chaos in
209 these findings is a result of experimental design and infection procedures. Those studies will
210 need to be done with other fungal pathogens, such as those entomopathogenic fungi that have
211 co-evolved with insects and are thus able to naturally infect the larvae without the need for
212 injection or other forced traumatic inoculation.
213 Another possibility is that a chaotic signature does exist in this system, but the results
214 are a false negative and its detection was hindered by limitations in the available data and the
215 method used. Chaotic dynamics can be highly sensitive to initial conditions and may require a
216 sufficiently large and high-resolution dataset to capture subtle fluctuations that signify chaotic
217 behavior. If the dataset is too sparse, contains significant observational gaps, or lacks a
218 sufficiently long time series, any underlying chaotic patterns may remain undetected or appear

219 as weak signals obscured by noise. Further data collection with higher temporal resolution and
220 greater replication may help clarify whether chaotic signatures are present but undetectable
221 under current conditions. Additionally, the inverse method employed for chaotic detection may
222 require refinement or revision to improve its accuracy in this specific biological context.
223 Different methods for identifying chaos, such as Lyapunov exponent analysis, recurrence
224 quantification analysis, or state-space reconstruction, may vary in their sensitivity to noise and
225 sampling limitations. Hence, it is possible that the analytic approach used here does not
226 adequately capture the nonlinear dynamics characteristic of fungal infections, particularly if
227 fungal-host interactions involve more complex regulatory feedback mechanisms than bacterial
228 infections. Future studies could explore alternative or complementary analytical techniques,
229 refining the methodological framework to better discern chaotic signatures in host-fungal
230 interactions.

231 An additional consideration when judging the implications of these findings for other
232 systems is our use of *G. mellonella.* Virulence in *G. mellonella* models of mutants or different
233 clinical isolates of the fungus *C. neoformans* corresponds to virulence in standard murine
234 models (8). While the *G. mellonella* model is good for assessing virulence through survival and
235 fungal burden assays, it lacks an adaptive immune response, which may lead to differences with
236 mammalian infection where the adaptive immune response is important. As of now, there are
237 no readily available inbred strains for this insect. While this reflects the situation for infection in
238 outbred populations it can also lead to variability between infected larvae depending on the
239 genetic differences between individuals. Phenotypic and genetic variability in hosts may lead to
240 noise in outcome measurements, resulting in chaotic signatures signal loss.

241 In summary, we developed a new method to study cryptococcal infection in *G.*
242 *mellonella* based on timelapse recording of the movement and pigmentation dynamics of
243 individual larvae, which provides a way to assess infection dynamics and disease progression at

244 high temporal resolution and in a high-throughput environment. Analysis of the mortality
245 outcomes from cryptococcal infection yielded deterministic non-chaotic dynamics with the
246 caveat that we cannot rule out the existence of non-apparent chaotic dynamics.
247

248 **Methods**

249 ***Galleria mellonella Infections***

250 Final instar *Galleria mellonella* larvae were obtained from Vanderhoorst Wholesale Inc.
251 (St. Mary's, OH, USA). Larvae were left to acclimate overnight in weighing boats. Larvae were
252 then injected with 10^6 cells of *C. neoformans* strain H99 suspended in PBS into the left rear
253 proleg using a 1 mL insulin needle 28 ½ gauge and Stepper Injector. The average volume
254 delivered to each larvae was 10 µl. Larvae were then placed into 24-well plates and kept at
255 room temperature.

256 ***Survival Recordings***

257 Timelapse imaging of the infected larvae was performed at room temperature over 10
258 days. Pairs of 12- or 24-well plates were imaged with a Brinno TLC130 Time Lapse Camera,
259 positioned from above using a clamp stand with the capture rate set to once every 15 minutes
260 (Supplementary Figure 1). Following the completion of the experiment, the timelapse images
261 were transferred and viewed using FIJI (ImageJ) (17). Control survival determinations, where
262 survival was determined by movement following physical stimulus with a pipette tip, were
263 performed concurrently.
264

265 ***Movement Analysis***

266 Timelapse movies were viewed on FIJI (ImageJ) so that each frame could be analyzed
267 individually (17). We manually scanned through the movement of each larva and recorded

268 frame after which no further movement was observed. This was recorded as the time at which
269 movement stopped. To obtain hour of death, the frame number was divided by four.
270
271 ***Melanization Analysis and Quantification***
272 Timelapse movies were processed on FIJI (ImageJ) (17) with each frame analyzed
273 individually. We scanned through each frame of the timelapse and recorded the frame in which
274 melanization was first seen occurring in the larvae. This was recorded as the time that
275 melanization occurred.
276 To further quantify the dynamics of melanization within the larvae, each of the wells in
277 the 24-well plate were selected using the circular selection tool in FIJI and added as different
278 Regions of Interest (ROIs) using the ROI Manager tool. The multi measure tool was selected,
279 which then measured the mean gray value of each well during each of the timelapse frames.
280 From this, we can see a sharp drop in mean gray value associated with the onset and
281 acceleration of melanization within the larvae.
282
283 **The inversion measure on a time distribution**
284 Given a distribution of time points, we first construct a histogram. For naturally discrete
285 time points, as in our simulated waiting times derived from chaotic or stochastic processes,
286 each unique time point serves as a bin. For continuous processes, we partition the distribution
287 into n bins based on a chosen parameter n.
288 Given a histogram with n bins, each containing an integer count, we first introduce a
289 small uniform random noise between 0 and ϵ ($\epsilon < 1$) to break ties while preserving the relative
290 order of distinct counts. Next, we partition the bins into consecutive, non-overlapping groups of
291 four, discarding any remainder. For each sequence x_1, x_2, x_3, x_4, we define
292 a **countertrend** (or **inversion**) as occurring when $(x_4 - x_1)$ and $(x_3 - x_2)$ share the same sign

(both positive or both negative). We then compute the proportion of sequences exhibiting inversions. Since this frequency is influenced by the randomness of the tie-breaking step, we repeat the process 1000 times with different randomizations and report the average.

To compute a p-value for the inversion measure, we performed a bootstrap test against the null hypothesis that the histogram is smooth. We considered two types of null densities: **kernel-smoothed** and **locally linear**.

For kernel smoothing, we applied MATLAB's built-in ksdensity function to the sample histogram. For the locally linear null density, we linearized the histogram as follows: for each consecutive sequence of four bins, let x_1, x_2, x_3, x_4represent the corresponding whole-number values. We fit a line of best fit for x_i as a function of ii and use this line as the null density for that sequence. If any fitted values fall below zero, we reset them to zero. Repeating this process for all sequences of four bins results in a piecewise linear null density, which is then normalized to sum to one.

To generate a bootstrap sample from a null density (either kernel-smoothed or locally linear), we draw the same number of samples as in the original histogram and recalculate the inversion measure. This procedure is repeated 1,000 times to create a bootstrapped null distribution of the inversion measure. We then computed a t-statistic and its corresponding p-value by comparing the observed inversion measure to this null distribution.

For the *Galleria* datasets, where some observations were not recorded at regular intervals, we addressed gaps by redistributing events as follows: whenever one or more observations were missing, we uniformly distributed the next observed count of events across the interval between the most recent and prior observations. A histogram was then constructed from this redistributed data, and the inversion measure was computed as before.

Since the redistribution process introduces randomness, we repeated it 1,000 times, generating a sample distribution of inversion measures. For each of these 1,000 histograms, we

318 conducted a bootstrap procedure with a sample size of 1,000, ultimately producing a null
319 distribution composed of 1,000,000 inversion measures. Using these distributions, we
320 estimated the p -value by calculating the probability that the sample inversion measure was
321 greater than or equal to a value drawn from the null distribution.

322 **Data availability**

323 Survival data used in this analysis and mean gray value measurements are deposited on
324 FigShare under the DOI:10.6084/m9.figshare.28616303

325 **Acknowledgements**

326 D.F.Q.S. is supported by NIH T32 AI 0074170-29. A.C. and D.F.Q.S are supported in part by R01
327 AI152078, R01 HL059842, and AI052733. A.B. was supported in part by NIH R01-CA164468 and
328 R01-DA033788. Biorender was used to produce Supplementary Figure 1.

329

330 **References:**

331 1. Casadevall A, Pirofski L. 2009. Virulence factors and their mechanisms of action: the view
332 from a damage–response framework. Journal of Water and Health 7:S2–S18.

333 2. Casadevall A. 2017. The Pathogenic Potential of a Microbe. mSphere 2:e00015-17.

334 3. Cobey KD, Ebrahimzadeh S, Page MJ, Thibault RT, Nguyen P-Y, Abu-Dalfa F, Moher D.
335 2024. Biomedical researchers' perspectives on the reproducibility of research. PLOS
336 Biology 22:e3002870.

337 4. Sella Y, Broderick NA, Stouffer KM, McEwan DL, Ausubel FM, Casadevall A, Bergman A.
338 2024. Preliminary evidence for chaotic signatures in host-microbe interactions. mSystems
339 9:e01110-23.

340 5. Garcia-Solache MA, Izquierdo-Garcia D, Smith C, Bergman A, Casadevall A. 2013. Fungal
341 Virulence in a Lepidopteran Model Is an Emergent Property with Deterministic Features.
342 mBio 4:10.1128/mbio.00100-13.

343 6. Smith DFQ, Casadevall A. 2022. On the relationship between Pathogenic Potential and
344 Infective Inoculum. PLOS Pathogens 18:e1010484.

345 7. F. Q. Smith D, Casadevall A. 2021. Fungal immunity and pathogenesis in mammals versus
346 the invertebrate model organism Galleria mellonella. Pathogens and Disease 79.

347 8. Mylonakis E, Moreno R, Khoury JBE, Idnurm A, Heitman J, Calderwood SB, Ausubel FM,
348 Diener A. 2005. Galleria mellonella as a Model System To Study Cryptococcus neoformans
349 Pathogenesis. Infection and Immunity 73:3842–3850.

350 9. Garcia-Bustos V, Ruiz-Saurí A, Ruiz-Gaitán A, Sigona-Giangreco IA, Cabañero-Navalon MD,
351 Sabalza-Baztán O, Salavert-Lletí M, Tormo MÁ, Pemán J. 2021. Characterization of the
352 Differential Pathogenicity of Candida auris in a Galleria mellonella Infection Model.
353 Microbiology Spectrum 9:e00013-21.

354 10. Kavanagh K, Fallon JP. 2010. Galleria mellonella larvae as models for studying fungal
355 virulence. Fungal Biology Reviews 24:79–83.

356 11. Firacative C, Khan A, Duan S, Ferreira-Paim K, Leemon D, Meyer W. 2020. Rearing and
357 Maintenance of Galleria mellonella and Its Application to Study Fungal Virulence. J Fungi
358 (Basel) 6:130.

359 12. Firacative C, Duan S, Meyer W. 2014. Galleria mellonella Model Identifies Highly Virulent
360 Strains among All Major Molecular Types of Cryptococcus gattii. PLOS ONE 9:e105076.

361 13. Camilotti E, Furian ,Thales Quedi, Borges ,Karen Apellanis, Ortiz Granados ,Oscar
362 Fernando, Zottis Chitolina ,Gabriela, de Brites Weber ,Thaína, Tonini da Rocha ,Daniela,
363 Nascimento ,Vladimir Pinheiro do, Souza Moraes ,Hamilton Luiz de, and Salle CTP. 2024.
364 Galleria mellonella larvae as an alternative model to determine the pathogenicity of avian
365 pathogenic Escherichia coli. Avian Pathology 53:507–519.

366 14. García-Carnero LC, Clavijo-Giraldo DM, Gómez-Gaviria M, Lozoya-Pérez NE, Tamez-
367 Castrellón AK, López-Ramírez LA, Mora-Montes HM. 2020. Early Virulence Predictors
368 during the Candida Species–Galleria mellonella Interaction. 3. Journal of Fungi 6:152.

369 15. Stempinski PR, Smith DFQ, Casadevall A. 2022. Cryptococcus neoformans Virulence Assay
370 Using a Galleria mellonella Larvae Model System. Bio Protoc 12:e4480.

371 16. Smith DFQ, Dragotakes Q, Kulkarni M, Hardwick JM, Casadevall A. 2022. Galleria
372 mellonella immune melanization is fungicidal during infection. 1. Commun Biol 5:1–13.

373 17. Schindelin J, Arganda-Carreras I, Frise E, Kaynig V, Longair M, Pietzsch T, Preibisch S,
374 Rueden C, Saalfeld S, Schmid B, Tinevez J-Y, White DJ, Hartenstein V, Eliceiri K, Tomancak
375 P, Cardona A. 2012. Fiji: an open-source platform for biological-image analysis. 7. Nature
376 Methods 9:676–682.

377

378

379 **Figure Legends**

380 ***Figure 1. Timelapse imaging can be used to record G. mellonella movement as a proxy for***
381 ***survival*. A.** The use of cessation of movement and time of melanization as a proxy for larval
382 death is consistent with the gold standard of manually checking the larvae every 24 h with a
383 physical stimulus. Camera movement survival data was rounded to nearest 24 h increment.
384 Manual survival group has an n = 24, while the group with survival quantified from the camera
385 timelapse movement has n = 168. **B.** Survival of larvae in a 12-well plate is improved compared
386 to those kept in a 24-well plate. All groups in Panel B have n = 24. P-values represent log-rank
387 Mantel-Cox comparisons

388

389 ***Figure 2. C. neoformans* infection of *G. mellonella* at high temporal resolution shows two**
390 **phases of infection. A.** Using timelapse photography, *G. mellonella* larval survival following
391 infection with *C. neoformans* was monitored in increments of 15 minutes, and time cessation of
392 movement and onset of melanization was recorded for each larva. This showed a two-phase
393 survival curve with one large phase of death occurring at 48 h and another slower phase after
394 96 h. **B.** The appearance of these two phases is lost when the temporal resolution is lowered to
395 every 24 h. For H99 infections, n = 864, while the PBS-injected n = 216.

396

397 ***Figure 3. G. mellonella* larvae show different characteristic melanization responses upon**
398 **infection. A.** Larvae that die during the first phase of death show onset of the melanization
399 response approximately 5 h prior to the larvae stop moving, while those at later time points
400 have more mixed patterns of melanization, often with pigmentation occurring hours after the
401 larvae stop moving. **B.** The difference between melanization and cessation of movement in the
402 first 48 h (n = 459) is different than the value for deaths occurring after 48 h (n=405). Statistical
403 significance was determined through an unpaired t-test, **** represents p<0.0001. **C.** Larvae

404 from the first phase of death show a sharp decline in mean gray value, which indicates rapid
405 production of black melanin pigment, **(D)** while larvae from the second phase of death show a
406 later and more gradual reduction in the mean gray value. **Panels C and D** are representative
407 quantifications of mean gray value for 3 separate larvae. Red arrows indicate time at which the
408 respective larvae stopped moving. **E.** Representative images of a larva that died in the first
409 phase of death compared to a larva from the second phase of death. Note that for early phase
410 there is continued larval movement following the onset of melanization, while the larva in the
411 second death phase does not move following melanization onset. White arrow indicates spot in
412 which melanization began from.
413
414 ***Figure 4. Death of G. mellonella larvae following C. neoformans infection does not***
415 ***demonstrate chaotic signatures****.* **(A).** The inversion method using bootstrap for locally linear
416 approximation of the distributions (histograms) was applied. The red line represents the actual
417 inversion measure of the distribution. No statistical significance was found, indicating no clear
418 evidence of chaotic behavior. (**B).** Histogram comparing the null (blue) and sample (orange-red)
419 distributions of the inversion measure. Inversion measure was performed through analysis of
420 842 larval death events.
421
422 ***Supplementary Figure 1. Timelapse photography set up.*** Timelapse camera is suspended
423 above two 24-well plates containing *G. mellonella* larvae using a 3-pronged clamp attached to a
424 support base.
425
426

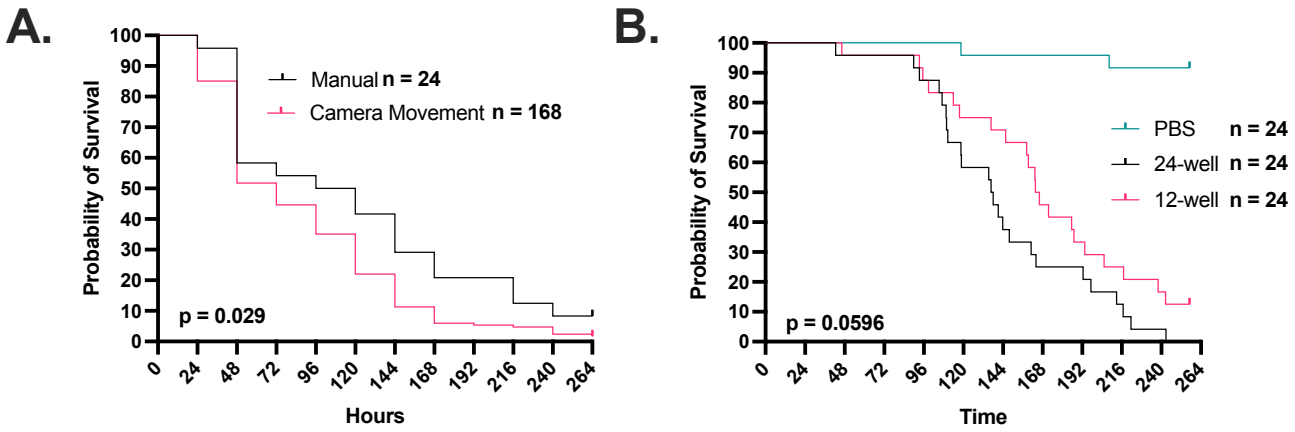

Figure 1. Timelapse imaging can be used to record G. mellonella movement as a proxy for survival. **A.** The use of cessation of movement and time of melanization as a proxy for larval death is consistent with the gold standard of manually checking the larvae every 24 h with a physical stimulus. Camera movement survival data was rounded to nearest 24 h increment. Manual survival group has an n = 24, while the group with survival quantified from the camera timelapse movement has n = 168. **B.** Survival of larvae in a 12-well plate is improved compared to those kept in a 24-well plate. All groups in Panel B have n = 24. P-values represent log-rank Mantel-Cox comparisons

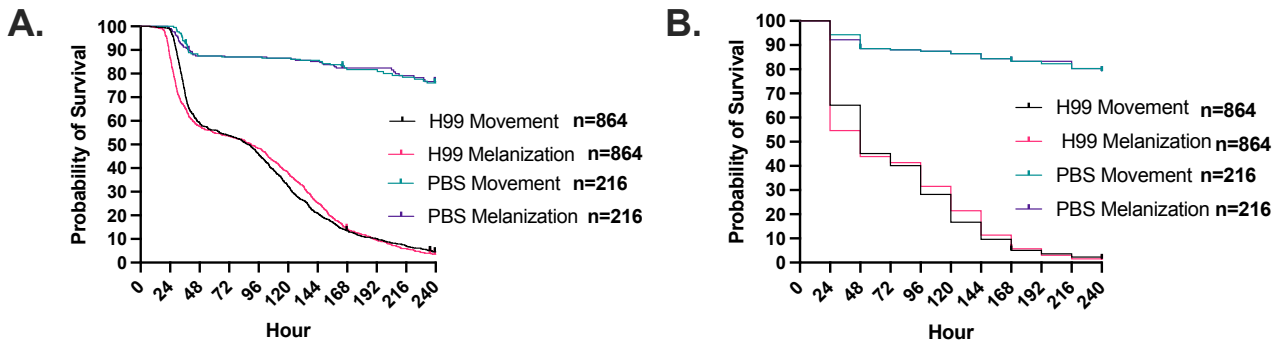

***Figure 2. C. neoformans* infection of *G. mellonella* at high temporal resolution shows two phases of infection. A.** Using timelapse photography, *G. mellonella* larval survival following infection with *C. neoformans* was monitored in increments of 15 minutes, and time cessation of movement and onset of melanization was recorded for each larva. This showed a two-phase survival curve with one large phase of death occurring at 48 h and another slower phase after 96 h. **B.** The appearance of these two phases is lost when the temporal resolution is lowered to every 24 h. For H99 infections, n = 864, while the PBS-injected n = 216.

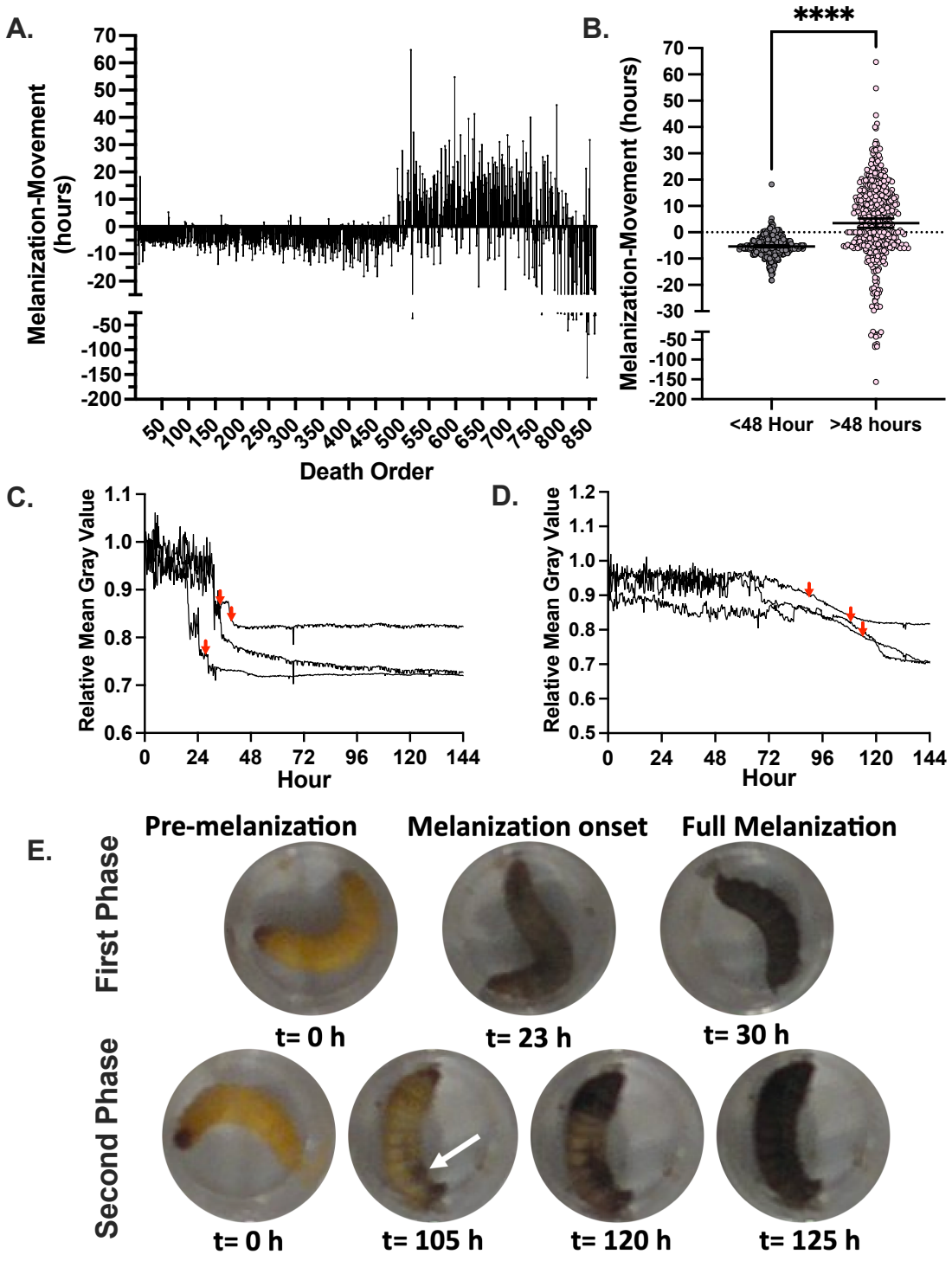

***Figure 3. G. mellonella* larvae show different characteristic melanization responses upon infection. A.** Larvae that die during the first phase of death show onset of the

melanization response approximately 5 h prior to the larvae stop moving, while those at later time points have more mixed patterns of melanization, often with pigmentation occurring hours after the larvae stop moving. **B.** The difference between melanization and cessation of movement in the first 48 h (n = 459) is different than the value for deaths occurring after 48 h (n=405). Statistical significance was determined through an unpaired t-test, **** represents $p<0.0001$. **C.** Larvae from the first phase of death show a sharp decline in mean gray value, which indicates rapid production of black melanin pigment, **(D)** while larvae from the second phase of death show a later and more gradual reduction in the mean gray value. **Panels C and D** are representative quantifications of mean gray value for 3 separate larvae. Red arrows indicate time at which the respective larvae stopped moving. **E.** Representative images of a larva that died in the first phase of death compared to a larva from the second phase of death. Note that for early phase there is continued larval movement following the onset of melanization, while the larva in the second death phase does not move following melanization onset. White arrow indicates spot in which melanization began from.

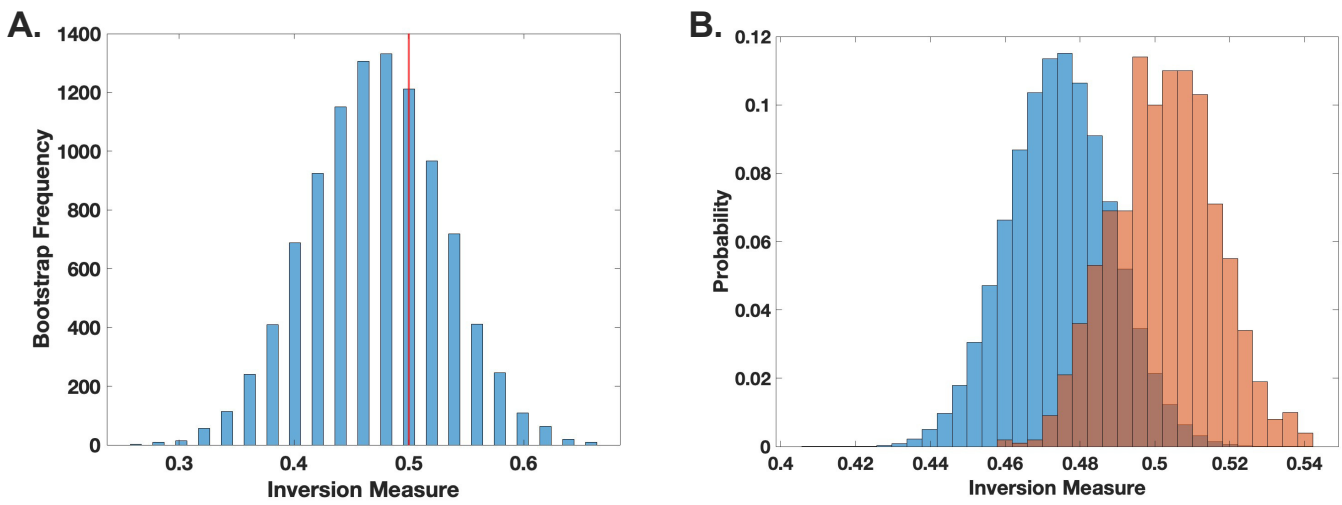

Figure 4. Death of G. mellonella larvae following C. neoformans infection does not demonstrate chaotic signatures. **(A).** The inversion method using bootstrap for locally linear approximation of the distributions (histograms) was applied. The red line represents the actual inversion measure of the distribution. No statistical significance was found, indicating no clear evidence of chaotic behavior. (**B).** Histogram comparing the null (blue) and sample (orange-red) distributions of the inversion measure. Inversion measure was performed through analysis of 842 larval death events.

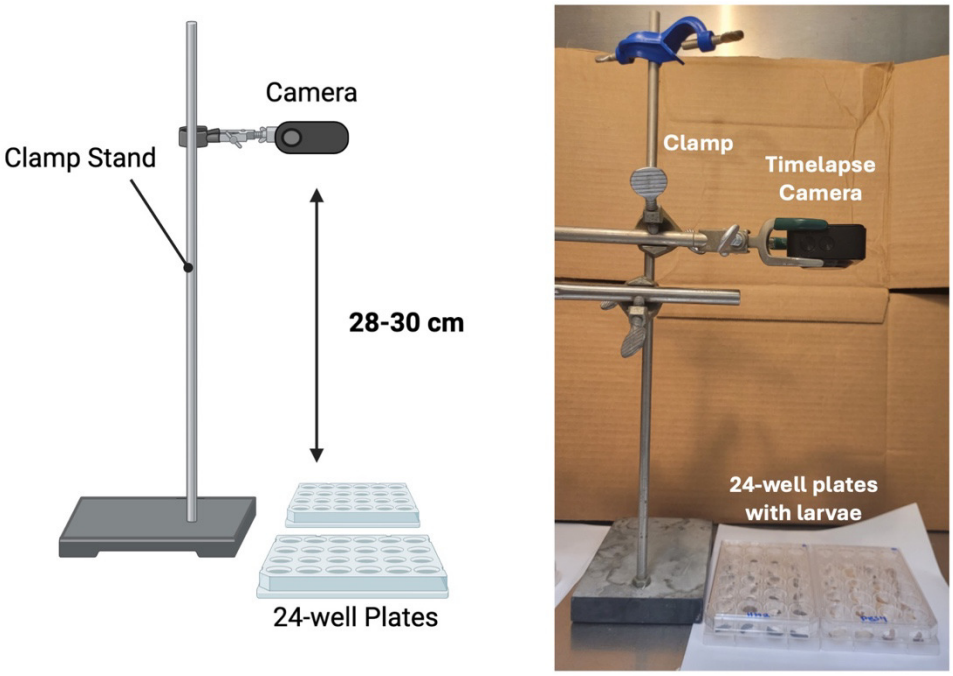

Supplementary Figure 1. Timelapse photography set up. Timelapse camera is suspended above two 24-well plates containing *G. mellonella* larvae using a 3-pronged clamp attached to a support base.